Surfaces and Interfaces 23 (2021) 100934

Contents lists available at ScienceDirect

Surfaces and Interfaces

journal homepage: www.sciencedirect.com/journal/surfaces-and-interfaces

Self-powered transparent photodetectors for broadband applications

Thanh Tai Nguyen [a,b], Malkeshkumar Patel [a,b], Joondong Kim [a,b,*]

[a] Photoelectric and Energy Device Application Lab (PEDAL), Multidisciplinary Core Institute for Future Energies (MCIFE)
[b] Department of Electrical Engineering, Incheon National University, 119 Academy Rd. Yeonsu, Incheon, 22012, Republic of Korea

ARTICLE INFO

Keywords:
Transparent photodetector
Self-powered operation
Broadband photodetector
Inorganic photoelectric device
Metal oxide

ABSTRACT

Broadband transparent photodetectors are achieved through the formation of a metal oxide heterojunction. A high transmittance of 66.63% for visible light (400–800 nm) results from the wide energy bandgaps of TiO_2 (3 eV) and NiO (3.86 eV). The metal-oxide heterojunction generates a photovoltaic effect due to the high open-circuit voltage (0.4 V), which spontaneously drives the NiO/TiO_2 photodetector for self-powered operations. Therefore, the transparent NiO/TiO_2 photodetector exhibits a self-operation mode with a fast response time (0.1 ms) while providing a high responsivity (0.43 A W^{-1}) and detectivity (8.6×10^9 Jones) without any external bias. Extreme cycle testing (over 20,000 times) was performed to confirm the high stability of the transparent NiO/TiO_2 photodetector. The proposed photovoltaic device can be an invisible power generator itself and be adopted for transparent optoelectronics, such as sensors, imaging, and memory applications with its self-operation mode.

Introduction

Transparent photoelectric technologies convert incident light into electrical energy without hindering human vision. Transparent features enable emerging see-through applications such as solar cells, neuromorphic computing, phototransistors, and light-emitting diodes [1–5]. In particular, transparent photosensors have been realized as a platform in smart windows, image processing, and optical communications [6–8]. Various semiconductor materials and device architectures have been exploited to develop high-functioning transparent photodetectors (TPDs) [9–12]. The majority of TPDs operate via electron excitation from wide bandgap materials by absorbing high-energy photons ($h\nu > 3$ eV, ultraviolet (UV) light). Such UV TPDs are indispensable in UV-based communication systems [6] and environmental monitoring [13].

Recently, extensions to TPD operations beyond the UV region have gained great interest in the research community. Multi-color detection with TPDs enables advanced broad spectral switches and memory storage applications [14,15]. The rapid progress of a high absorption coefficient and broadband photosensitized materials, including layered structures [16–18], perovskites [14], quantum dot [19] and ternary organic semiconductors [20–22]have made great contributions to enhanced broadband photodetector performances in term of responsivity, light spectra detection range, and response speed. For example, Zijin et al. enhanced the performance of PDs via investigating photomultiplication phenomena of organic semiconductors [23], resulting in improving photogenerated charges collection, characterized by external quantum efficiency [24], and extending light spectra response. In regard of efficient TPDs, it is important to satisfy the 5-S criteria of a PD(sensitivity, speed, stability, signal-to-noise ratio, and spectral selectivity) [9,10]. Creating a built-in potential (V_{in}) for a PD is desired to satisfy these requirements [25]. Furthermore, a sufficiently high V_{in} magnitude can drive TPD operations without an external power supply. Self-powered PDs are not only energy-efficient but also highly preferable for the progress of integrated circuit technologies [6,26].

Different strategies have been developed to obtain self-powered PDs, including Schottky junctions, heterojunctions, and homojunctions [6,27,28]. However, multi-functional PDs are needed to satisfy optical transparency, self-powered operations, and broadband photodetection. This report presents a self-powered PD formed via a metal-oxide heterojunction. The wide energy bandgap of TiO_2 ($E_g \geq 3$ eV) enables a highly transparent optical device based on an NiO layer. The heterojunction formation between NiO and TiO_2 simultaneously generates the photovoltaic effect from differences in their Fermi energies. The self-operation of the transparent NiO/TiO_2 PD provides a high responsivity (0.43 A W^{-1}) and detectivity (8.6×10^9 Jones) without any applied external bias. In addition, extreme cycling tests confirm the stability of the transparent PD. The features of the TiO_2-based transparent optoelectronic provide the possibility of transparent photovoltaics, broadband

* Corresponding author
E-mail address: joonkim@incheon.ac.kr (J. Kim).

https://doi.org/10.1016/j.surfin.2021.100934
Received 1 November 2020; Received in revised form 14 December 2020; Accepted 6 January 2021
Available online 10 January 2021

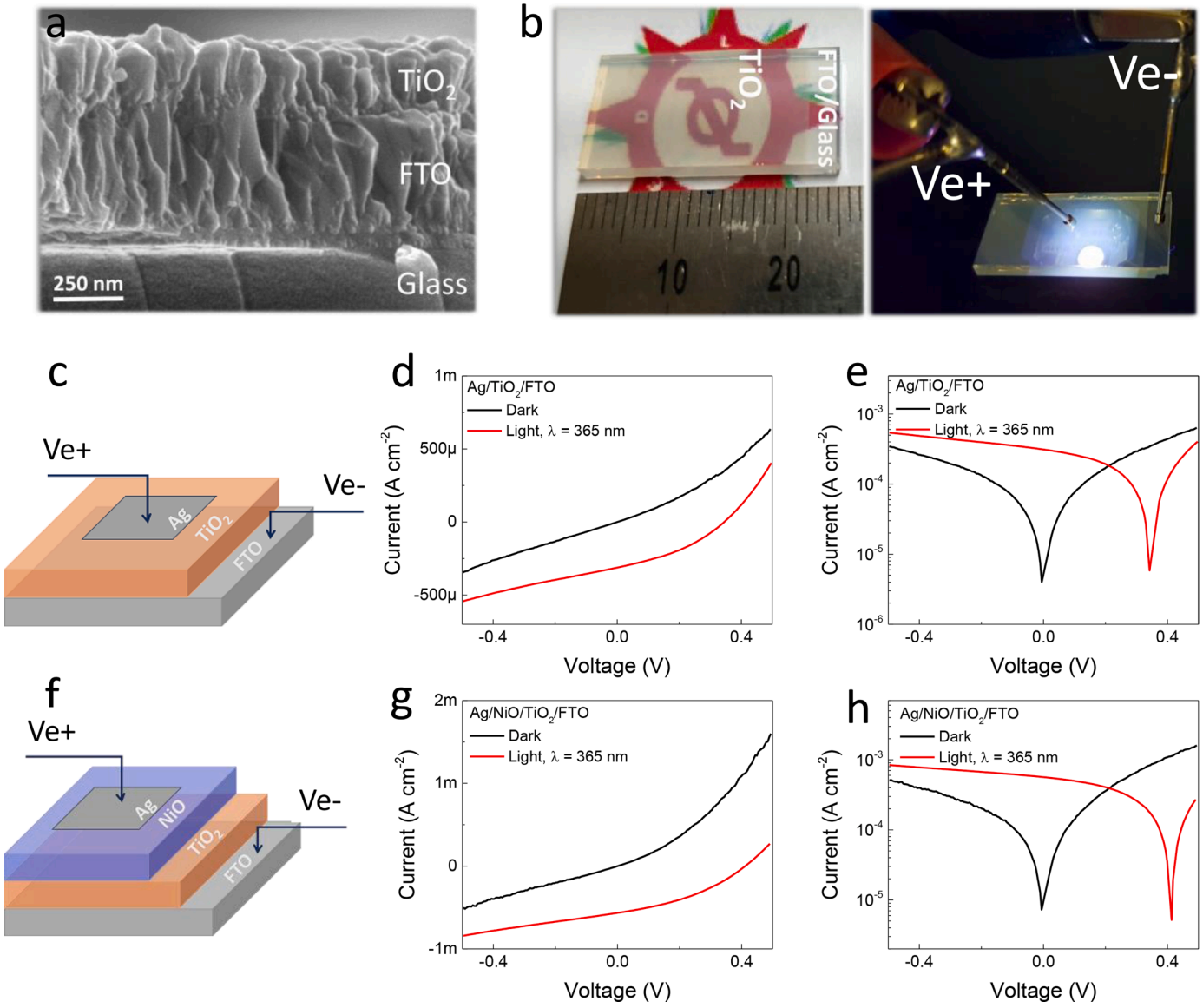

Fig. 1. (a) SEM image of TiO_2/FTO/Glass. (b) Photography of transparent TiO_2 based photodetectors. Schematic of the TiO_2-based transparent photodetectors, (c) Ag/TiO_2/FTO and (f) Ag/NiO/TiO_2/FTO. Current-voltage characteristics of the Ag/TiO_2/FTO device in (d) linear and (e) semi-log scales. Current-voltage characteristics of the Ag/NiO/TiO_2/FTO device in (g) linear and (h) semi-log scales.

photosensing, and photoelectric applications.

Experimental section

Prior to metal-oxide deposition, fluorine-doped tin oxide-coated (FTO) glass substrates (735159 Aldrich, sheet resistance 7 Ω/□) were cleaned with a sequence of acetone, methanol, and deionized water under ultra-sonication for 10 min and then dried with nitrogen gas flow. The rutile TiO_2 layer was prepared in two steps: DC sputtering of Ti and oxidation of the Ti layer by rapid thermal processing (RTP). The Ti was DC sputtered (SNTEK, Korea) using a Ti target (iTASCO, purity 99.99%). During sputtering, a DC power of 300 W was applied to the Ti target for 5 min with a uniform Ar flow (50 sccm) to keep maintain a pressure of 5 mTorr. To form the Rutile TiO_2, the Ti/FTO/glass was thermally oxidized in the RTP system at 600°C for 15 min. Then, the fabricated TiO_2/FTO/glass was annealed at 600°C in Ar for 15 min in the RTP system. The NiO film was sputtered for 10 min using a Ni target (iTASCO, purity 99.99%) with an Ar/O_2 flow rate of 20/5 sccm at a DC power of 50 W and working pressure of 3 mTorr. The base pressure of 3 $\times 10^{-6}$ Torr was achieved prior to sputtering. Pre-sputtering for 10 min was performed while rotating the substrate at 5 rpm to ensure film uniformity.

Cross-sectional images of the NiO/TiO_2/FTO structure were obtained using field emission scanning electron microscopy (FE-SEM, JEOL, JSM_7001F). The current-voltage characteristics of the TiO_2-based TPD were measured using a potentiostat/galvanostat (PGStat, ZIVE SP2, WonA Tech). We applied linear sweep voltammetry with a positive scan direction at a rate of 100 mV s^{-1}. A light source from 365 to 640 nm was used to measure the device performances. The transient photocurrent profiles were obtained using various LED sources coupled with a function generator (MFG-3013A, MCH Instrument), which were recorded using the PGStat (Chronoamperometry, zero bias). The donor concentration (N_D) of TiO_2 and the flat-band potential of TiO_2 based TPD devices were determined through analyzing the Mott-Schottky characteristics which was obtained by potentiodynamic impedance spectroscopy measurement. The potentiodynamic impedance spectroscopy was performed from an initial potential of -1 V to a final potential of 0.2 V at a step size of 25 mV, AC amplitude of 10 mV, initial frequency of 1 MHz, and final frequency of 0.1 Hz (log sweep) and the measurements were performed at normal speed. The Mott-Schottky data was

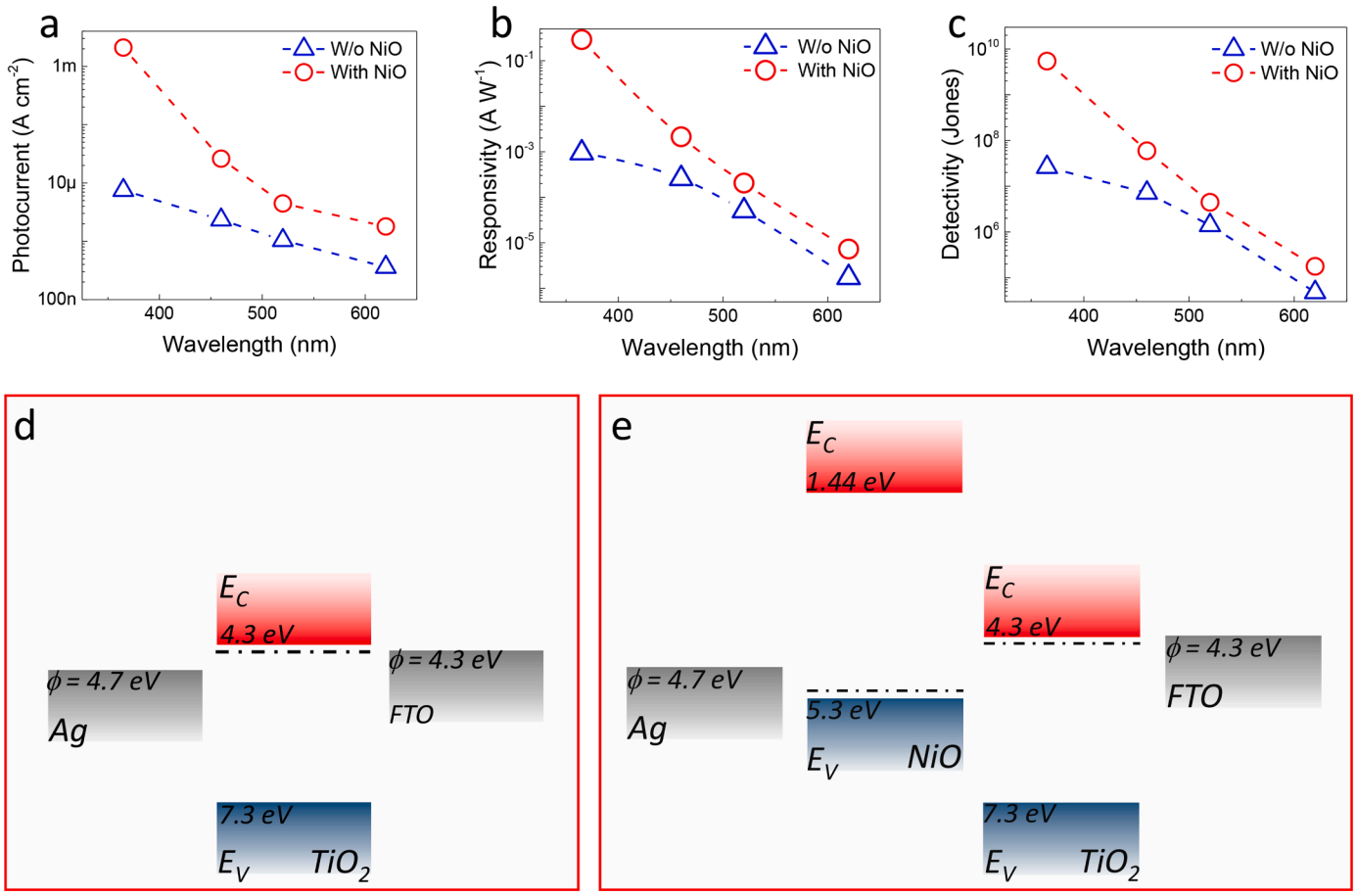

Fig. 2. Spectral response of the TiO_2-based TPD: (a) photocurrent, (b) responsivity, and (c) detectivity. Energy band diagram of the (d) Ag/TiO_2/FTO and (e) Ag/NiO/TiO_2/FTO.

obtained at frequency of 2.5 kHz.

Result and discussion

Fig. 1a presents cross-sectional SEM images of the TiO_2/FTO/glass sample, which confirm the formation of the TiO_2 layer on the FTO/glass substrate. The thickness of the TiO_2 is approximately 120 nm. The large scale TiO_2/FTO/glass sample is highly transparent with see-through features, as shown in Fig. 2b. Two kinds of transparent PDs were prepared to investigate the photo-reactive TiO_2 layer. The bare TiO_2 device was prepared from a TiO_2 layer on FTO-coated glass as the bottom electrode. Meanwhile, a top electrode was formed from an Ag point contact above the TiO_2 layer. Distinct from the bare TiO_2 device, the NiO/TiO_2 device has a heterojunction between the p-type NiO and n-type TiO_2. The device schematics are illustrated in Fig. 1c and f. Here, TiO_2 functions as the primary light-absorbing layer to generate electron-hole pairs. The FTO and Ag were connected to negative and positive terminals, respectively, to collect photogenerated electrons and holes. Initially, the electrical properties of the TiO_2-based PD were characterized by current-voltage (I-V) profiles of devices under dark and illuminated conditions. Fig. 1d and g presents linear-scale I-V curves of the Ag/TiO_2/FTO and Ag/NiO/TiO_2/FTO under identical measurement conditions. Both devices exhibit non-symmetric dark I-V behaviors, indicating the formation of a built-in potential inside the devices. Under UV illumination ($\lambda = 365$ nm), the TiO_2-based PDs display a distinct difference between the dark and illuminated I-V curves over the entire measured bias range. The photo-gain, which is defined as the ratio of the photocurrent to the dark current at zero bias, is approximately 78. This confirms the self-operating feature of the fabricated TiO_2-based PD, which favors developing small and portable photoelectric applications.

Furthermore, the devices gave a photoresponse when in the photovoltaic mode. The photovoltaic effect is induced by transitions between light and current flow. Photons are quanta of the smallest discrete amount of light and produce electron-hole pairs in the light-reactive layer. The existing electric field inside the space charge region separates and collects the carriers. As a result, the accumulation of electrons causes a split of the Fermi-level to produce the open-circuit voltage (V_{OC}) of a solar cell, which can be applied as the driving power for general electronic devices. The bare TiO_2 device has a V_{OC} of 0.34 V, while the improved value of 0.4 V is achieved from the NiO/TiO_2 device, as shown in Fig. 1e and h, respectively. While some previous research has been reported for TiO_2-based PDs [6,29,30], the photovoltaic effect has not been studied.

The effects of the NiO layer on the performance of TiO_2-based PDs were further investigated under illumination of intermittent light for broad spectral applications. The photocurrent–time characteristics of the Ag/TiO_2/FTO and Ag/NiO/TiO_2/FTO without an applied bias are presented in Fig. S1. The enhanced photocurrent is not only observed in the UV region but also in the visible region, as illustrated in Fig. 2a. Under pulsed UV illumination ($\lambda = 365$ nm), the Ag/TiO_2/FTO gave a response with a current density of 7.5 μA cm^{-2}. Meanwhile, this value was greatly increased to 2.4 mA cm^{-2} with an NiO-embedded device, which accounts for improvements by factor of 320. In the visible region, the photocurrent enhanced by factors of 11.2, 4.3, and 5 for wavelengths of 460, 520, and 620 nm, respectively. The visible light response of TiO_2 can be achieved through different approaches, including integration with low bandgap materials, metal or nonmetal doping, hot electron transitions for embedded noble metals, and self-doped TiO_2 (Ti^{3+} state

formation) [31–34]. Here, without introducing low bandgap semiconductors and metal/nonmetal elements, the visible light response of TiO_2-based PDs are attributed to hot electron transitions or Ti^{3+} state formation. To clarify the origin of the visible response of TiO_2-based PDs, the photoresponse of NiO/TiO_2/FTO samples under different monochromatic wavelengths were analyzed for various top-contact schemes, as shown in Fig. S2. Interestingly, a broadband response was obtained for all contact schemes, which demonstrates the independence of the UV-Visible response for TiO_2 as hot electron transitions to metal contacts [33]. That is, the Ti^{3+} state formation is believed to be the origin of visible light detection in TiO_2-based PDs.

Due to improvements in photocurrent, TiO_2-based PDs with an NiO insertion can detect light signals with a greater responsivity and detectivity, which are key parameters to evaluate the PD quality. The responsivity (R) and detectivity (D) can be estimated from the following relations,

$$R = \frac{I_{ph}}{P_{light}}$$

$$D = \frac{R}{\sqrt{2qI_d}}$$

Where I_{ph}, P_{light}, q, and I_d are the photocurrent, incident light intensity, elementary charge and dark current, respectively. According to Fig. 2b and c, the Ag/NiO/TiO_2/FTO device responded to UV light with R and D values of 0.26 A W^{-1} and 5.4 × 10^9 Jones, respectively. Meanwhile, the values were only 0.94 mA W^{-1} and 2.6 × 10^7 Jones for the Ag/TiO_2/FTO device (UV light intensity of 8 mW cm^{-2}). The NiO embedded device obtained the highest response in the visible region at a wavelength of 460 nm. For a light intensity of 9.1 mW cm^{-2} (λ = 460 nm), the device gave R and D values of 2.9 mA W^{-1} and 5.9 × 10^7 Jones, respectively. These indicate an enhancement by factor of 11.2 for R and 8.3 for D compared with the sole TiO_2 device (R and D values of 0.26 mA W^{-1} and 7.2 × 10^6 Jones). It is noted that the broadband photoresponse of the TiO_2-based PD was obtained under zero bias. In addition, light spectra response of TiO_2 based photodetectors were further characterized by incident photon to electron conversion efficiency (IPCE). IPCE was estimated by the relation,

$$IPCE = \frac{1240 \times J_{SC}\ (mA\ cm^{-2})}{\lambda(nm) \times light\ intensity\ (mW\ cm^{-2})} \times\ 100\%$$

Where, J_{SC}, λ are photocurrent density and light wavelength, respectively. The Ag/NiO/TiO_2/FTO device exhibited higher IPCE value, compared to Ag/TiO_2/FTO device, for the entire light detecting range, as shown in Fig. S3. Moreover, the NiO/TiO_2 based device can respond to broader light spectra with wavelength detecting limit of 850 nm. Meanwhile, the device with sole TiO_2 just detected light spectra up to wavelength of 620 nm, presented by Fig. S3.

The transparency of photoelectric devices are commonly determined by average visible transmittance parameter, AVT [35]. The AVT can be estimated by the following formula, [2]

$$\mathrm{AVT} = \frac{\int_{380\ nm}^{825\ nm} T(\lambda)P(\lambda)S(\lambda)d\lambda}{\int_{380\ nm}^{825\ nm} P(\lambda)S(\lambda)d\lambda}$$

Where, λ is the wavelength, T is the transmission, P is the photopic response of human eye and S is the solar photon flux. The NiO/TiO_2 combination exhibits a high visible transmittance with AVT of 66.63% (Fig. S4), suggesting it is a promising candidate for transparent optoelectronic applications.

Energy diagrams were proposed for the Ag/TiO_2/FTO and Ag/NiO/TiO_2/FTO devices to better understand the dynamic behaviors of photogenerated carriers inside TiO_2-based PDs. The conduction band of TiO_2 is 4.3 eV [36], which is higher than the work function of Ag (ϕ_{Ag} = 4.7 eV) and equals the value for FTO, as shown in Fig. 2d. This indicates a Schottky barrier formation at the TiO_2/Ag interface, which is evidenced by the non-linear dark I-V characteristics of the Ag/TiO_2/FTO device shown in Fig. 1a. The energy barrier height at the Ag/TiO_2 Schottky interface is 0.4 eV for the Ag/TiO_2/FTO device, which increases significantly to 2.9 eV by inserting the NiO layer to create a heterostructure with the TiO_2, as illustrated in Fig. 2e. The NiO/TiO_2 structure forms a staggered junction type, which is essential for photogenerated charge separation processes [37]. The possibility of a Schottky junction at the Ag/NiO interface is ruled out from the linear I-V curve for the Ag/NiO/FTO sample, as shown in Fig. S5. When light is illuminated onto TiO_2-based PDs, photogenerated electron-hole pairs are generated in the TiO_2 and separated by the electric-field-induced Schottky junction (Ag/TiO_2) and heterojunction (NiO/TiO_2). The higher energy barrier height allows the NiO/TiO_2 junction to separate and collect photogenerated charges more effectively compared to the Ag/TiO_2 Schottky contact, which results in a higher PD performance, as shown in Fig. 2b and c.

In addition to physical models, the properties of the Ag/TiO_2 and NiO/TiO_2 junctions were further characterized in terms of their built-in potential and width of the space charge region. The built-in potential (V_{in}) was estimated by extrapolating the $(A/C_{SC})^2$ curves to the voltage axis for the Mott-Schottky characterizations, which belong to the Ag/TiO_2/FTO and Ag/NiO/TiO_2/FTO devices, where A is the device active area and C_{SC} is the capacitance. The Mott-Schottky profiles of the devices are presented in Fig. S6. The V_{in} for TiO_2-based PDs with and without NiO are 0.45 and 0.24 eV, respectively. A higher V_{in} indicates a stronger electric field at the junction interface of the NiO/TiO_2 structure compared to the Ag/TiO_2 Schottky contact. The space charge region width (W_{SCR}) is another decisive parameter for efficient charge collection. The upward trend of the ($(A/C_{SC})^2$ – V) relation dominates the Mott-Schottky characteristics of the Ag/NiO/TiO_2/FTO device, as presented in Fig. S5 b. This indicates a much lower carrier concentration in TiO_2 as compared with NiO [38]. The donnor concentration of TiO_2 (N_D) can be estimated from the Mott-Schottky slope of the Ag/TiO_2/FTO device as,

$$N_D = \frac{2}{q\varepsilon_r\varepsilon_0 A^2}\frac{dV}{d\left(1/C^2\right)}$$

where ε_0 and ε_r are the vacuum dielectric constant (8.854 × 10^{-12} F m^{-1}) and TiO_2 dielectric constant (55), respectively [29]. The estimated N_D of TiO_2 is 1.14 × 10^{17} cm^{-3}, which is lower than the reported carrier concentration of NiO ($N_A = 1.8 \times 10^{19}$) [39]. Therefore, the W_{SCR} can be estimated from the simplified relation [40,41],

$$W_{SCR} = \sqrt{\frac{2\varepsilon_0\varepsilon_{rV_{in}}}{qN_D}}$$

Thus, the W_{SCR} of the Ag/TiO_2 Schottky junction and NiO/TiO_2 heterojunction are 15 and 21 nm, respectively. The Ag/NiO/TiO_2/FTO device shows a wider W_{SCR} compared with Ag/TiO_2/FTO. Therefore, it has a higher probability to collect photogenerated electron-hole pairs, which leads to an enhanced photocurrent. The W_{SCR} behaviour of NiO/TiO_2 heterojunction was further investigated by characterizing $(1/C_{SC})^2$-V relationship for different ultraviolet light intensities, as shown in Fig. S7. Under illuminating condition, $(1/C_{SC})^2$ value decreased with the increase of light intensities. This indicates the increase of device capacitance, resulting from the decrease of space region width under light illuminating conditions [42,43].It is noted that the NiO/TiO_2 responds to incident wavelengths with a sharp spike transient photocurrent signal, which was not observed for the sole TiO_2-based device, as shown in Fig. S1. Under visible light illumination, the photogenerated holes can be trapped by the Ti^{3+} states [44]. The accumulation of trapped holes can induce local electric field which make disturbance of built-in electric field at junction interface [45,46]. The sudden change of junction electric field may cause the spike in the transient photocurrent of device

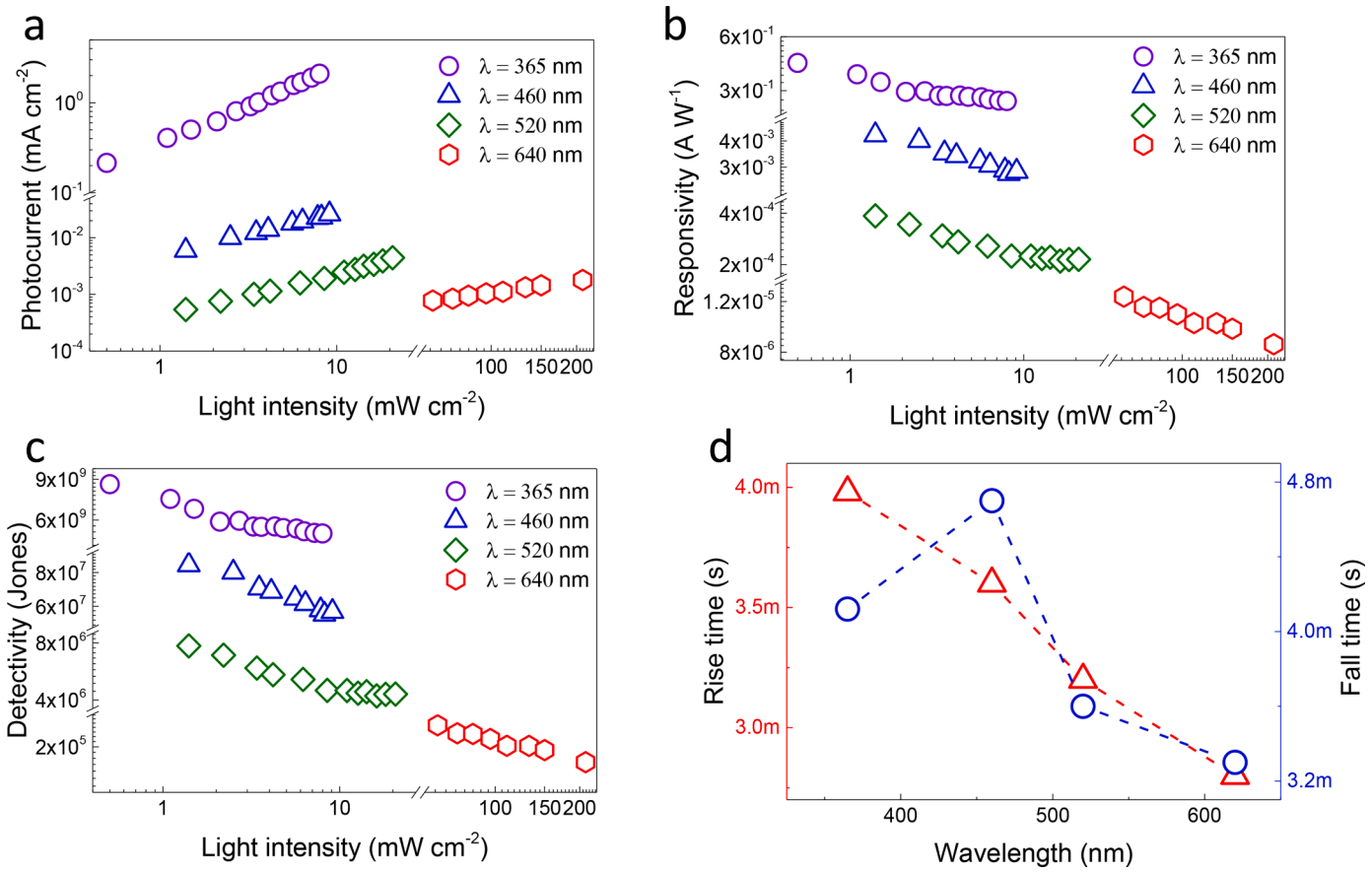

Fig. 3. Spectral response of the Ag/NiO/TiO_2/FTO as dependent on the light intensity: (a) photocurrent, (b) responsivity, and (c) detectivity. (d) Response speed of the Ag/NiO/TiO_2/FTO device for broadband illumination.

under on-off states of illuminated light [6,47]. The wavelength-induced spike magnitude is attributed to the relative position of the Ti^{3+} states to the space charge region [48]. Hence, a larger W_{SCR} (corresponding to NiO/TiO_2) is more easily affected by trapped carriers compared to the narrower W_{SCR} (corresponding to Ag/TiO_2), which results in different transient photocurrent shapes.

The reliability of broadband photodetection in transparent NiO/TiO_2-based PDs was examined by characterizing the response of the devices to variations in the incident light intensity. All characterizations were conducted at zero-bias conditions. A higher photocurrent at a larger light intensity is observed for broad wavelengths (UV-Visible), as presented in Fig. 3a. At higher incident light powers, more carriers will be generated inside the device. The upward trend of the photocurrent indicates the capability of NiO/TiO_2 heterojunction to effectively split and collect photogenerated carriers. This also suggests the high sensitivity of the device to a wide range of light intensities. Fig. 3b and c show the responsivity and detectivity profiles for the Ag/NiO/TiO_2/FTO devices, respectively. In contrast to photocurrent trends, increasing the light intensity results in a decreased responsivity and detectivity over all the detected wavelengths, which is attributed to the complex process of photogenerated carrier traps or recombination inside the device [29]. Transparent NiO/TiO_2 heterostructures detected wavelengths of 365, 460, 520, and 620 nm with responsivities of 0.43 A W^{-1} (P_{light} of 0.5 mW cm^{-2}), 4.3 mA W^{-1} (P_{light} of 1.4 mW cm^{-2}), 0.39 mA W^{-1} (P_{light} of 1.4 mW cm^{-2}), and 12 μA W^{-1} (P_{light} of 62.3 mW cm^{-2}), respectively. The corresponding detectivities were 8.6 × 10^9, 8.5 × 10^7, 7.7 × 10^6, and 2.5 × 10^5 Jones.

Stability is one of the critical parameters for practical applications of broadband transparent PDs [49]. The photoresponse of transparent NiO/TiO_2 heterostructures to different wavelengths under on-off states was recorded for several thousand cycles, as presented in Fig. 4. The device exhibited a clear difference in current between the off and on states of incident light after 20,000 cycles for all detected wavelengths, which strongly confirms the stability of the NiO/TiO_2 heterostructure. The NiO/TiO_2-based PD can detect broadband light at rapid speeds. The photodetection rise and fall times of the device are less than 5 ms for the entire UV-Visible spectra, as shown in Fig. 3d. Table 1 summaries the performance of transparent NiO/TiO_2 photodetector for broadband of light illumination at zero-biased condition. Furthermore, the progress of the PD based on TiO_2 as well as various broadband PDs based on different photoactive materials is presented by Table 2. The photoresponse speed from this work is among the fastest PDs, which operate over a broad spectrum. Moreover, the NiO/TiO_2 heterostructure is transparent with a transmittance of 66.63%, suggesting NiO/TiO_2 is a promising candidate for high-speed transparent optoelectronic applications. Fast respond speed of a photodetector can be achieved via applying unique device structure, selecting suitable photosensitive materials or utilizing specific phenomena of semiconductor materials for photodetecting application. Huajing et al. achieved ultraviolet photoresponse speed with ns time unit by deploying asymmetric Shottky junctions based transparent AgNW/TiO_2/FTO structure [6]. Amit et al. obtained broadband, fast photoresponse speed (81/179 μs) by utilizing pyro-photoelectric of ZnO which is well-developed for high speed photodetectors [50]. Through optimizing vertical, layered structure of $PtSe_2$ which possesses high carrier mobility, Long-Hui et al. succeeded in obtaining μs photoresponse with opaque device [51]. Herein, the TiO_2-based photodetector detects broadband light wavelengths (λ = 365 – 620 nm) at zero-biased condition without scarifying transparency. In regard of TiO_2 based photodetector progress, this work achieves fast photoresponse speed (rise and fall time are less than 5 ms) with excellent

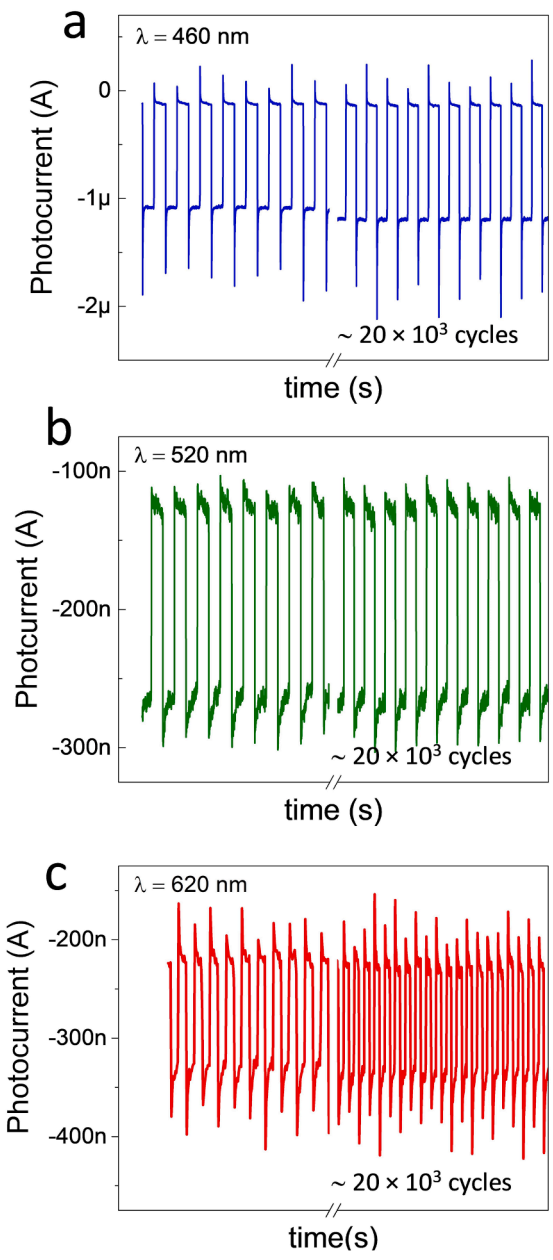

Fig. 4. Stability testing of the NiO/TiO_2-based photodetector under different illumination conditions: (a) 460, (b) 520, and (c) 620 nm.

Table 1
Summarization of the performance of transparent NiO/TiO_2 photodetector for broadband of light illumination at zero-biased condition, including responsivity (R), detectivity (D), rise time (τ_r) and fall time (τ_f).

Wavelength (nm)	R (A W^{-1})	D (Jones)	τ_r (ms)	τ_f (ms)
365	0.43	8.6×10^9	3.9	4.1
460	4.3×10^{-3}	8.5×10^7	3.6	4.7
520	0.4×10^{-3}	7.7×10^6	2.3	3.6
620	12×10^{-6}	2.5×10^5	2.8	3.3

responsivity in ultraviolet light region (0.43 A W^{-1}), attributed to the developed electric filed at NiO/TiO_2 heterojunction interface. The sufficiently high built-in potential (V_{bi} = 0.45 eV) that develops at the NiO/TiO_2 interface can efficiently separate photogenerated electron-hole pairs inside the TiO_2. These separated photogenerated carriers will immediately drift away from the depletion region towards the electrodes due to the electric field, which results in a rapid photoresponse of the device [6,25,52]. Faster response speed can be obtained

Table 2
Summarization for the progress of TiO_2-based PDs and the performance of various broadband PDs based on different photoactive materials, including the transmittance (T), responsivity (A W^{-1}), rise time (τ_r), and fall time (τ_f).

	Spectra range	Bias (V)	T (%)	R (A W^{-1})	τ_r /τ_f	Illumination	Ref.
TiO_2/TiO_x	UV	0	-	6×10^{-3}	< 0.1/0.1 s	λ = 365 nm	[29]
TiO_2	UV	0	-	42×10^{-6}	1.2/7.1 s	λ = 350 nm	[27]
TiO_2	UV	0	70	33×10^{-3}	44 ns/1.85 μs	λ = 350 nm	[6]
Co_3O_4/TiO_2	UV-Vis[1]	5	73	2.4	0.17/0.21 s	λ = 620 nm	[53]
Co_3O_4/ZnO	UV-NIR[2]	0	76	12.9×10^{-3}	81.7/179 μs	White light	[50]
Cu_2O/ZnO	Vis	0	73	0.28×10^{-3}	0.15/0.15 s	1 Sun	[54]
$PtSe_2$/GaAs	UV-NIR	0	-	0.26	5.5 /6.5 μs	λ = 808 nm	[51]
Se/n-Si	UV-Vis	-2	-	37.4×10^{-3}	48 s	λ = 610 nm	[55]
TiO_2/$MAPbI_3$ QDs	UV-NIR	1	85	0.2	7/4 s	λ = 700 nm	[56]
CdS/P3HT	UV-NIR	0	-	10.5×10^{-3}	200/200 s	λ = 780 nm	[57]
Perovskite/CuO	UV-NIR	0	-	7.3×10^{-3}	300/300 ms	λ = 1000 nm	[58]
TiO_2	UV-Vis	0	66.63	0.43, 4.3×10^{-3}, 0.4×10^{-3}, 12×10^{-6}	3.9/4.1 ms, 3.6/4.7 ms, 2.3/3.6 ms, 2.8/3.3 ms	λ = 365 nm, λ = 460 nm, λ = 520 nm, λ = 620 nm	This Work

[1] Visible
[2] Near infrared.

by reducing TiO_2 thickness [6], however, it will reduce the light absorption, resulting in low responsivity value.

Conclusion

Transparent and self-operational PDs are realized using metal-oxide heterojunctions. The large energy bandgaps of NiO and TiO_2 give an overall transmittance of 66.63% over visible wavelengths for the designed PDs. The TPD can operate in a self-operation mode due to the photovoltaic effect of metal-oxide devices. The devices show a high stability as confirmed by over 20,000 cycling operations. Light conversion to electric power was observed from the NiO/TiO_2 PD via the staggered heterojunction formation. This transparent NiO/TiO_2 PD showed a high-performing responsivity (0.43 A W^{-1}) and detectivity (8.6×10^9 Jones) with a fast response time of 5 ms. Moreover, the TiO_2-based device can broaden photodetection for broad wavelengths based on the formation of Ti^{3+} states. The multi-functional NiO/TiO_2 heterojunction PD is recommended for its high transparency, broadband photodetection, long-stability, and self-powered operation. This suggests a promising approach to develop energy-efficient, environmentally friendly, and stable transparent optoelectronic devices.

Declaration of Competing Interest

There is no conflict of interest on this manuscript of "**Self-powered transparent photodetectors for broadband applications**" by Thanh Tai Nguyen et al. to be considered for publication in Surfaces and Interfaces.

Creadit author statements

T. Nguyen performed the experimental works. T. M. Patel visualized the result. Nguyen and M. Patel wrote the draft. J. Kim conceived the method.

Acknowledgements

The authors acknowledge the financial support through the National Research Foundation (NRF-2020R1A2C1009480, 2020H1D3A2A02085884 and 2020R1I1A1A01068573) by the Ministry of Education of Korea and Korea Institute of Energy Technology Evaluation and Planning (KETEP-20203030010310) of Korea (Republic of).

References

[1] S. Kim, M. Patel, T.T. Nguyen, J. Yi, C.P. Wong, J. Kim, Si-embedded metal oxide transparent solar cells, Nano Energy 77 (2020), 105090.
[2] C.J. Traverse, R. Pandey, M.C. Barr, R.R. Lunt, Emergence of highly transparent photovoltaics for distributed applications, Nat. Energy. 2 (2017) 849–860.
[3] P.K. Yang, W.Y. Chang, P.Y. Teng, S.F. Jeng, S.J. Lin, P.W. Chiu, J.H. He, Fully transparent resistive memory employing graphene electrodes for eliminating undesired surface effects, Proc. IEEE. 101 (2013) 1732–1739.
[4] H. Cho, J.-M. Choi, S. Yoo, Highly transparent organic light-emitting diodes with a metallic top electrode: The dual role of a Cs2CO3 layer, Opt. Express. 19 (2011) 1113.
[5] K. Nomura, H. Ohta, K. Ueda, T. Kamiya, M. Hirano, H. Hosono, Thin-film transistor fabricated in single-crystalline transparent oxide semiconductor, Science 300 (2003) 1269–1272 (80-.).
[6] H. Fang, C. Zheng, L. Wu, Y. Li, J. Cai, M. Hu, X. Fang, R. Ma, Q. Wang, H. Wang, Solution-processed self-powered transparent ultraviolet photodetectors with ultrafast response speed for high-performance communication system, Adv. Funct. Mater. 29 (2019), 1809013.
[7] M. Hossain, G.S. Kumar, S.N. Barimar Prabhava, E.D. Sheerin, D. McCloskey, S. Acharya, K.D.M. Rao, J.J. Boland, Transparent, flexible silicon nanostructured wire networks with seamless junctions for high-performance photodetector applications, ACS Nano 12 (2018) 4727–4735.
[8] S. Huang, C.F. Guo, X. Zhang, W. Pan, X. Luo, C. Zhao, J. Gong, X. Li, Z.F. Ren, H. Wu, Buckled tin oxide nanobelt webs as highly stretchable and transparent photosensors, Small 11 (2015) 5712–5718.
[9] J. Chen, W. Ouyang, W. Yang, J.H. He, X. Fang, Recent progress of heterojunction ultraviolet photodetectors: Materials, integrations, and applications, Adv. Funct. Mater. 30 (2020), 1909909.
[10] F. Teng, K. Hu, W. Ouyang, X. Fang, Photoelectric detectors based on inorganic p-type semiconductor materials, Adv. Mater. 30 (2018), 1706262.
[11] C. Xie, X.T. Lu, X.W. Tong, Z.X. Zhang, F.X. Liang, L. Liang, L.B. Luo, Y.C. Wu, Recent progress in solar-blind deep-ultraviolet photodetectors based on inorganic ultrawide bandgap semiconductors, Adv. Funct. Mater. 29 (2019), 1806006.
[12] S. Gunasekaran, D. Thangaraju, R. Marnadu, J. Chandrasekaran, T. Alshahrani, M. Shkir, A. Durairajan, M.P.F. Graça, M. Elango, Fabrication of high-performance SiO2@p-CuO/n-Si core-shell structure based photosensitive diode for photodetection application, Surfaces and Interfaces 20 (2020), 100622.
[13] X. Xu, J. Chen, S. Cai, Z. Long, Y. Zhang, L. Su, S. He, C. Tang, P. Liu, H. Peng, X. Fang, A real-time wearable UV-radiation monitor based on a high-performance p-CuZnS/n-TiO2 photodetector, Adv. Mater. 30 (2018), 1803165.
[14] X. Hu, X. Zhang, L. Liang, J. Bao, S. Li, W. Yang, Y. Xie, High-performance flexible broadband photodetector based on organolead halide perovskite, Adv. Funct. Mater. 24 (2014) 7373–7380.
[15] Z. Zheng, L. Gan, H. Li, Y. Ma, Y. Bando, D. Golberg, T. Zhai, A fully transparent and flexible ultraviolet-visible photodetector based on controlled electrospun ZnO-CdO heterojunction nanofiber arrays, Adv. Funct. Mater. 25 (2015) 5885–5894.
[16] C.H. Liu, Y.C. Chang, T.B. Norris, Z. Zhong, Graphene photodetectors with ultra-broadband and high responsivity at room temperature, Nat. Nanotechnol. 9 (2014) 273–278.
[17] V. Dhyani, P. Dwivedi, S. Dhanekar, S. Das, High performance broadband photodetector based on MoS2/porous silicon heterojunction, Appl. Phys. Lett. 111 (2017), 191107.
[18] S.S. Hegde, A.G. Kunjomana, P. Murahari, B.K. Prasad, K. Ramesh, Vacuum annealed tin sulfide (SnS) thin films for solar cell applications, Surfaces and Interfaces 10 (2018) 78–84.
[19] S.W. Shin, K.H. Lee, J.S. Park, S.J. Kang, Highly transparent, visible-light photodetector based on oxide semiconductors and quantum Dots, ACS Appl. Mater. Interfaces. 7 (2015) 19666–19671.

[20] Z. Zhao, J. Wang, J. Miao, F. Zhang, Photomultiplication type organic photodetectors with tunable spectral response range, Org. Electron. 69 (2019) 354–360.
[21] X. Zhou, D. Yang, D. Ma, A. Vadim, T. Ahamad, S.M. Alshehri, Ultrahigh gain polymer photodetectors with spectral response from UV to Near-Infrared using ZnO nanoparticles as anode interfacial layer, Adv. Funct. Mater. 26 (2016) 6619–6626.
[22] A. Armin, R.D. Jansen-Van Vuuren, N. Kopidakis, P.L. Burn, P. Meredith, Narrowband light detection via internal quantum efficiency manipulation of organic photodiodes, Nat. Commun. 6 (2015) 6343.
[23] J. Miao, M. Du, Y. Fang, F. Zhang, Acceptor-free photomultiplication-type organic photodetectors, Nanoscale 11 (2019) 16406–16413.
[24] Z. Zhao, C. Xu, L. Niu, X. Zhang, F. Zhang, Recent progress on broadband organic photodetectors and their applications, Laser Photonics Rev 14 (2020), 2000262.
[25] L. Zheng, K. Hu, F. Teng, X. Fang, Novel UV–Visible photodetector in photovoltaic mode with fast response and ultrahigh photosensitivity employing Se/TiO2 nanotubes heterojunction, Small 13 (2017), 1602448.
[26] Z.L. Wang, Self-powered nanosensors and nanosystems, Adv. Mater. 24 (2012) 280–285.
[27] L. Zheng, F. Teng, Z. Zhang, B. Zhao, X. Fang, Large scale, highly efficient and self-powered UV photodetectors enabled by all-solid-state n-TiO2 nanowell/p-NiO mesoporous nanosheet heterojunctions, J. Mater. Chem. C. 4 (2016) 10032.
[28] Y. Wang, P. Wang, Y. Zhu, J. Gao, F. Gong, Q. Li, R. Xie, F. Wu, D. Wang, J. Yang, Z. Fan, X. Wang, W. Hu, High performance charge-transfer induced homojunction photodetector based on ultrathin ZnO nanosheet, Appl. Phys. Lett. 114 (2019), 011103.
[29] Y. Gao, J. Xu, S. Shi, H. Dong, Y. Cheng, C. Wei, X. Zhang, S. Yin, L. Li, TiO2 nanorod arrays based self-powered UV photodetector: Heterojunction with NiO nanoflakes and enhanced UV photoresponse, ACS Appl. Mater. Interfaces. 10 (2018) 11269–11279.
[30] J. Xu, W. Yang, H. Chen, L. Zheng, M. Hu, Y. Li, X. Fang, Efficiency enhancement of TiO2 self-powered UV photodetectors using a transparent Ag nanowire electrode, J. Mater. Chem. C. 6 (2018) 3334–3340.
[31] G. Wang, X. Xiao, W. Li, Z. Lin, Z. Zhao, C. Chen, C. Wang, Y. Li, X. Huang, L. Miao, C. Jiang, Y. Huang, X. Duan, Significantly enhanced visible light photoelectrochemical activity in TiO2 nanowire arrays by nitrogen implantation, Nano Lett 15 (2015) 4692–4698.
[32] W. Wang, Y. Liu, J. Qu, Y. Chen, M.O. Tadé, Z. Shao, Synthesis of hierarchical TiO2-C3N4 hybrid microspheres with enhanced photocatalytic and photovoltaic activities by maximizing the synergistic effect, ChemPhotoChem 1 (2017) 35–45.
[33] F.P. García De Arquer, A. Mihi, D. Kufer, G. Konstantatos, Photoelectric energy conversion of plasmon-generated hot carriers in metal-insulator-semiconductor structures, ACS Nano 7 (2013) 3581–3588.
[34] S. Tan, Z. Xing, J. Zhang, Z. Li, X. Wu, J. Cui, J. Kuang, Q. Zhu, W. Zhou, Ti3+-TiO2/g-C3N4 mesostructured nanosheets heterojunctions as efficient visible-light-driven photocatalysts, J. Catal. 357 (2018) 90–99.
[35] Z. Hu, Z. Wang, F. Zhang, Semitransparent polymer solar cells with 9.06% efficiency and 27.1% average visible transmittance obtained by employing a smart strategy, J. Mater. Chem. A. 7 (2019) 7025–7032.
[36] D. Zhang, X. Gu, F. Jing, F. Gao, J. Zhou, S. Ruan, High performance ultraviolet detector based on TiO2/ZnO heterojunction, J. Alloys Compd. 618 (2015) 551–554.
[37] M.T. Uddin, Y. Nicolas, C. Olivier, W. Jaegermann, N. Rockstroh, H. Junge, T. Toupance, Band alignment investigations of heterostructure NiO/TiO2 nanomaterials used as efficient heterojunction earth-abundant metal oxide photocatalysts for hydrogen production, Phys. Chem. Chem. Phys. 19 (2017) 19279–19288.
[38] K. Yan, Z. Wei, T. Zhang, X. Zheng, M. Long, Z. Chen, W. Xie, T. Zhang, Y. Zhao, J. Xu, Y. Chai, S. Yang, Near-Infrared photoresponse of one-sided abrupt MAPbI3/TiO2 heterojunction through a tunneling process, Adv. Funct. Mater. 26 (2016) 8545–8554.
[39] M. Patel, H.S. Kim, J. Kim, All transparent metal oxide ultraviolet photodetector, Adv. Electron. Mater. 1 (2015), 1500232.
[40] H. Kim, J. Kim, E. Lee, D.W. Kim, J.H. Yun, J. Yi, Effect of the short collection length in silicon microscale wire solar cells, Appl. Phys. Lett. 102 (2013), 193904.
[41] R.F. Pierret, Semiconductor device fundamentals, First edit, Addison Wesley, New York, 1996.
[42] I. Mora-Seró, G. Garcia-Belmonte, P.P. Boix, M.A. Vázquez, J. Bisquert, Impedance spectroscopy characterisation of highly efficient silicon solar cells under different light illumination intensities, Energy Environ. Sci. 2 (2009) 678–686.
[43] I. Zonno, A. Martinez-Otero, J.C. Hebig, T. Kirchartz, Understanding Mott-Schottky measurements under illumination in organic bulk heterojunction solar cells, Phys. Rev. Appl. 7 (2017), 034018.
[44] T.L. Thompson, J.T. Yates, Surface science studies of the photoactivation of TiO2 - New photochemical processes, Chem. Rev. 106 (2006) 4428–4453.
[45] T. Dittrich, V. Zinchuk, V. Skryshevskyy, I. Urban, O. Hilt, Electrical transport in passivated Pt/TiO2/Ti Schottky diodes, J. Appl. Phys. 98 (2005), 104501.
[46] J. Shi, Y. Li, Y. Li, D. Li, Y. Luo, H. Wu, Q. Meng, From ultrafast to ultraslow: Charge-carrier dynamics of perovskite solar cells, Joule 2 (2018) 879–901.
[47] T. Tai, M. Patel, J. Kim, All-inorganic metal oxide transparent solar cells, Sol. Energy Mater. Sol. Cells. 217 (2020), 110708.
[48] X. Xin, T. Xu, J. Yin, L. Wang, C. Wang, Management on the location and concentration of Ti3+ in anatase TiO2 for defects-induced visible-light photocatalysis, Appl. Catal. B Environ. 176–177 (2015) 354–362.
[49] F. Teng, K. Hu, W. Ouyang, X. Fang, Photoelectric Detectors based on Inorganic P-type Semiconductor Materials, Adv. Mater. 30 (2018), 1706262.
[50] A.K. Rana, M. Patel, T.T. Nguyen, J.H. Yun, J. Kim, Transparent Co3O4/ZnO photovoltaic broadband photodetector, Mater. Sci. Semicond. Process. 117 (2020), 105192.
[51] L.H. Zeng, S.H. Lin, Z.J. Li, Z.X. Zhang, T.F. Zhang, C. Xie, C.H. Mak, Y. Chai, S. P. Lau, L.B. Luo, Y.H. Tsang, Fast, self-driven, air-stable, and broadband photodetector based on vertically aligned PtSe2/GaAs heterojunction, Adv. Funct. Mater. 28 (2018), 1705970.
[52] T.T. Nguyen, M. Patel, S. Kim, R.A. Mir, J. Yi, V.A. Dao, J. Kim, Transparent photovoltaic cells and self-powered photodetectors by TiO2/NiO heterojunction, J. Power Sources. 481 (2021), 228865.
[53] B. Choudhuri, A. Mondal, S.M.M.D. Dwivedi, M. Henini, Fabrication of novel transparent Co3O4-TiO2 nanowires p-n heterojunction diodes for multiband photodetection applications, J. Alloys Compd. 712 (2017) 7–14.
[54] C. De Melo, M. Jullien, Y. Battie, A.En Naciri, J. Ghanbaja, F. Montaigne, J. F. Pierson, F. Rigoni, N. Almqvist, A. Vomiero, S. Migot, F. Mücklich, D. Horwat, Semi-Transparent p-Cu2O/n-ZnO Nanoscale-film heterojunctions for photodetection and photovoltaic applications, ACS Appl. Nano Mater. 2 (2019) 4358–4366.
[55] W. Yang, K. Hu, F. Teng, J. Weng, Y. Zhang, X. Fang, High-performance silicon-compatible large-area UV-to-Visible broadband photodetector based on integrated lattice-matched type II Se/n-Si heterojunctions, Nano Lett 18 (2018) 4697–4703.
[56] Z. Zheng, F. Zhuge, Y. Wang, J. Zhang, L. Gan, X. Zhou, H. Li, T. Zhai, Decorating perovskite quantum dots in TiO2 nanotubes array for broadband response photodetector, Adv. Funct. Mater. 27 (2017), 1703115.
[57] X. Yu, H. Yin, H. Li, W. Zhang, H. Zhao, C. Li, M. Zhu, Piezo-phototronic effect modulated self-powered UV/visible/near-infrared photodetectors based on CdS: P3HT microwires, Nano Energy 34 (2017) 155–163.
[58] H. Sun, W. Tian, F. Cao, J. Xiong, L. Li, Ultrahigh-performance self-powered flexible double-twisted fibrous broadband perovskite photodetector, Adv. Mater. 30 (2018), 1706986.